Discontinuous Galerkin Methods for Mass Conservation Equations for Environmental Modeling

M.J. Guillot[a], B. Rivière[b], M.F. Wheeler[b]

[a]Department of Mechanical Engineering, University of New Orleans, 2000 Lakeshore Dr, New Orleans, LA 70148

[b]Center for Subsurface Modeling, TICAM, The University of Texas at Austin
Austin, TX 78712

A discontinuous Galerkin method is introduced for a system of time-dependent 3-D mass transport equations on unstructured meshes using hexahedral elements. Linear approximating functions are employed which are defined locally on each element, providing four degrees of freedom per element. In addition, we define a procedure for computing locally conservative velocities from fluxes defined on faces of elements. This implementation is validated on a series of test cases.

1. Introduction

In this paper a discontinuous Galerkin (DG) formulation is developed for the 3-D unsteady convection-diffusion equation. A unique property of this approach is that the DG solution satisfies the mass conservation equation locally element by element. In addition, the flexibility of DG methods is an attractive feature for dynamic h-p refinements, which include nonconforming adaptive meshes and variable local order of approximation. Moreover, because they are highly local, DG methods only require communication between elements which share faces; thus they are well-suited for parallel computation. The term DG method can refer to several finite element methods using discontinuous discrete spaces, such as the Bassi and Rebay method [1], the Local Discontinuous Galerkin (LDG) [2] method, the Oden, Babuska and Baumann method [3] the interior penalty Galerkin methods of Wheeler [4], Douglas and Dupont [5], and the NIPG methods [6,7]. In Arnold, Brezzi, Cockburn and Marini [8] a general framework of these methods is presented. Application of these methods to a wide variety of problems can be found in [9].

2. Model Problem Formulation

The basic form of the mass conservation equation for system of species in a domain Ω is

$$\begin{aligned} \frac{\partial C_i}{\partial t} + \nabla \cdot (C_i \boldsymbol{V}) &= \nabla \cdot (D \nabla C_i) + S_i(\mathbf{C}), \quad \text{in} \quad \Omega, \\ (C_i \boldsymbol{V} - D \nabla C_i) \cdot \boldsymbol{n} &= C_{D,i} \boldsymbol{V} \cdot \boldsymbol{n}, \quad \text{on} \quad \Gamma_{\text{in}}, \end{aligned}$$

$$D\nabla C_i \cdot \boldsymbol{n} \;=\; 0, \quad \text{on} \quad \Gamma_{\text{out}},$$

where C_i is the ith species partial density, S_i the external sources, $\boldsymbol{V}$ the velocity field and D the diffusion coefficient. The boundary of the domain is decomposed into an inflow part $\Gamma_{\text{in}} = \{\boldsymbol{x} \in \partial\Omega : \boldsymbol{V} \cdot \boldsymbol{n} < 0\}$ and an outflow part $\Gamma_{\text{out}} = \partial\Omega \setminus \Gamma_{\text{in}}$.

3. Discontinuous Galerkin Formulation

In this section we define both semi-discrete and discrete time approximations. We first establish notation. The domain Ω is subdivided into hexaedral elements $\{E\}_E$. Let Γ be the union of interior faces of elements. We associate with each set γ_k in Γ, a unit normal vector $\boldsymbol{n}_k$. For γ_k in $\partial\Omega$, the vector $\boldsymbol{n}_k$ is outward to $\partial\Omega$. The finite element subspace consists of discontinuous piecewise linear polynomials. We now define for any test function w, the average $\{w\}$, the jump $[w]$ and the upwind w_* values.

$$\{w\} = \frac{1}{2}(w|_{E_k^1}) + \frac{1}{2}(w|_{E_k^2}), \quad [w] = (w|_{E_k^1}) - (w|_{E_k^2}), \quad \forall \gamma_k = \partial E_k^1 \cap \partial E_k^2,$$

$$w_* = \begin{cases} w|_{E_k^1} & \text{if} \quad \boldsymbol{V} \cdot \boldsymbol{n}_k \geq 0, \\ w|_{E_k^2} & \text{if} \quad \boldsymbol{V} \cdot \boldsymbol{n}_k < 0. \end{cases}, \quad \forall \gamma_k = \partial E_k^1 \cap \partial E_k^2.$$

Based on the work in [11], we can formulate the semi-discrete scheme for a single specie and for convenience drop the subscript i:

$$\begin{aligned} \int_\Omega \frac{\partial C}{\partial t} w \;=\; & -\sum_{E\in\mathcal{E}_h} \int_E D\nabla C \cdot \nabla w + \sum_{E\in\mathcal{E}_h} \int_E \boldsymbol{V} C \cdot \nabla w + \int_\Omega S w \\ & + \sum_{\gamma_k \in \Gamma} \int_{\gamma_k} \{D\nabla C \cdot \boldsymbol{n}_k\}[w] - \sum_{\gamma_k \in \Gamma} \int_{\gamma_k} \{D\nabla w \cdot \boldsymbol{n}_k\}[C] \\ & - \sum_{\gamma_k \in \Gamma} \int_{\gamma_k} \boldsymbol{V} \cdot \boldsymbol{n}_k C_*[w] - \sum_{\gamma_k \in \Gamma_{\text{out}}} \int_{\gamma_k} \boldsymbol{V} \cdot \boldsymbol{n}_k C w - \sum_{\gamma_k \in \Gamma_{\text{in}}} \int_{\gamma_k} \boldsymbol{V} \cdot \boldsymbol{n}_k C_D w. \end{aligned}$$

The discretization in time is obtained by time lagging the flux terms corresponding to the vertical faces. This standard technique for solving surface water problems has the advantage of producing a block tridiagonal system. We write $\Gamma = \Gamma^{\text{HF}} \cup \Gamma^{\text{VF}}$, where Γ^{HF} is the union of the horizontal faces of the elements and Γ^{VF} the union of vertical faces. The fully discrete scheme is then:

$$\begin{aligned} & \int_\Omega C^{n+1} w + \Delta t \sum_{E\in\mathcal{E}_h} \int_E D\nabla C^{n+1} \cdot \nabla w - \Delta t \sum_{E\in\mathcal{E}_h} \int_E \boldsymbol{V} C^{n+1} \cdot \nabla w \\ & -\Delta t \sum_{\gamma_k \in \Gamma^{\text{HF}}} \int_{\gamma_k} \{D\nabla C^{n+1} \cdot \boldsymbol{n}_k\}[w] + \Delta t \sum_{\gamma_k \in \Gamma^{\text{HF}}} \int_{\gamma_k} \{D\nabla w \cdot \boldsymbol{n}_k\}[C^{n+1}] \\ & +\Delta t \sum_{\gamma_k \in \Gamma} \int_{\gamma_k} \boldsymbol{V} \cdot \boldsymbol{n}_k C_*^{n+1}[w] = \int_\Omega C^n w + \Delta t \int_\Omega S^n w \\ & + \sum_{\gamma_k \in \Gamma^{\text{VF}}} \int_{\gamma_k} \{D\nabla C^n \cdot \boldsymbol{n}_k\}[w] - \sum_{\gamma_k \in \Gamma^{\text{VF}}} \int_{\gamma_k} \{D\nabla w \cdot \boldsymbol{n}_k\}[C^n] \\ & - \sum_{\gamma_k \in \Gamma^{\text{VF}}} \int_{\gamma_k} \boldsymbol{V} \cdot \boldsymbol{n}_k C_*^n[w] - \sum_{\gamma_k \in \Gamma_{\text{out}}} \int_{\gamma_k} \boldsymbol{V} \cdot \boldsymbol{n}_k C^n w - \sum_{\gamma_k \in \Gamma_{\text{in}}} \int_{\gamma_k} \boldsymbol{V} \cdot \boldsymbol{n}_k C_D^n w. \end{aligned}$$

4. Velocity Field Approximation

In many applications such as environmental modeling of surface water, flux face values are only provided, e.g. environmental modeling using CE-QUAL-ICM [10]. In the DG method interior velocity distributions over each element are required. Here an approximation we developed given known flow rates across each edge plus the additional constraint of local mass conservation on each element is described. In order to approximate the velocity field, the hexahedral is divided into two prisms. The prisms are formed by projecting vertically in the direction. The velocity is assumed to vary as

$$\text{Prism 1} \begin{cases} v_x = a_1 + c_1(x - \bar{x}) \\ v_y = a_2 + c_1(y - \bar{y}) \end{cases} \qquad \text{Prism 2} \begin{cases} v_x = a_1 + c_1(x - \bar{x}) \\ v_y = a_2 + c_1(y - \bar{y}) \end{cases} \tag{1}$$

The above expressions involve eight unknowns which are found by considering the six known flow rates across each face, plus local conservation of mass on each prism expressed as, $\nabla \cdot \boldsymbol{V} = -(1/V_E)\partial V_E/\partial t \equiv -\delta$, where V_E is the volume of element E and δ is defined as the rate of increase of volume per unit volume. Let us define by $Q_1, \ldots, Q_4$ (resp. $\boldsymbol{n}_1, \ldots, \boldsymbol{n}_4$) the fluxes (resp. the outward normal vectors) over the vertical faces of the hexaedral E and Q_5, Q_6 (resp. $\boldsymbol{n}_5, \boldsymbol{n}_6$) the fluxes (resp. outward normal vectors) across the horizontal faces. A_i denotes the area of the face with flux Q_i. Substituting the velocity expressions given by (1) into the conservation equation yields the following values

$$c_1 = c_2 = \frac{-(Q_6 - Q_5)}{2V_E} - \frac{\delta}{2}, \quad c_3 = \frac{(Q_6 - Q_5)}{V_E}.$$

By writing $\boldsymbol{n}_i = (n_{x_i}, n_{y_i}, n_{z_i})$, the expressions for a_1, a_2, b_1 and b_2 are found to be

$$\begin{aligned}
a_1 &= \frac{\frac{Q_1}{A_1} n_{y_4} - \frac{Q_4}{A_4} n_{y_1}}{n_{x_1} n_{y_4} - n_{x_4} n_{y_1}} \\
&\quad + \frac{n_{y_1}(n_{x_4}(x_4 + x_1) + n_{y_4}(y_4 + y_1)) - n_{y_4}(n_{x_1}(x_1 + x_2) + n_{y_1}(y_1 + y_2))}{2c_1^{-1}(n_{x_1} n_{y_4} - n_{x_4} n_{y_1})} \\
a_2 &= \frac{\frac{Q_4}{A_4} n_{x_1} - \frac{Q_1}{A_1} n_{x_4}}{n_{x_1} n_{y_4} - n_{x_4} n_{y_1}} \\
&\quad + \frac{n_{x_4}(n_{x_1}(x_1 + x_2) + n_{y_1}(y_1 + y_2)) - n_{x_1}(n_{x_4}(x_4 + x_1) + n_{y_4}(y_4 + y_1))}{2c_1^{-1}(n_{x_1} n_{y_4} - n_{x_4} n_{y_1})} \\
a_3 &= \frac{\frac{Q_2}{A_2} n_{y_3} - \frac{Q_3}{A_3} n_{y_2}}{n_{x_2} n_{y_3} - n_{x_3} n_{y_2}} \\
&\quad + \frac{n_{y_2}(n_{x_3}(x_3 + x_4) + n_{y_3}(y_3 + y_4)) - n_{y_3}(n_{x_2}(x_2 + x_3) + n_{y_2}(y_2 + y_3))}{2c_1^{-1}(n_{x_2} n_{y_3} - n_{x_3} n_{y_2})} \\
a_4 &= \frac{\frac{Q_3}{A_3} n_{x_2} - \frac{Q_2}{A_2} n_{x_3}}{n_{x_2} n_{y_3} - n_{x_3} n_{y_2}} \\
&\quad + \frac{n_{x_3}(n_{x_2}(x_2 + x_3) + n_{y_2}(y_2 + y_3)) - n_{x_2}(n_{x_3}(x_3 + x_4) + n_{y_3}(y_3 + y_4))}{2c_1^{-1}(n_{x_2} n_{y_3} - n_{x_3} n_{y_2})}.
\end{aligned}$$

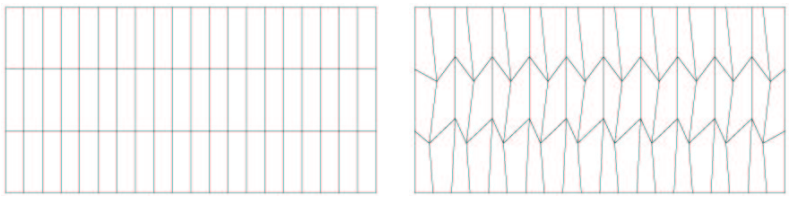

Figure 1. 60 element test case: (left) rectangular elements, (right) quadrilateral elements.

5. Validation

For simplicity we consider only a system of two equations, namely temperature and salinity.

5.1. One Dimensional Study

The initial conditions are uniform for both salinity and temperature with salinity set to $10gm/m^3$ and temperature set to 7^0C. The salinity at inflow boundaries is linearly ramped from 10 to 12 over a period of 1.5 days. The temperature at the inflow boundaries remains at 7^0C. However, the air temperature above the surface of the domain increases during the simulation. This provides a heat flux source at the surface of the domain which raises the temperature within the domain during the simulation. The first case is a simple 1D flow with diffusion set to zero. The flow enters the domain at $x = 0$ and exits at $x = 3.e^5m$. This solution was computed on three meshes. Each mesh was divided into $20x3x1$ elements. The first mesh was divided into rectangular elements and aligned with the coordinate directions, the second was divided into quadrilateral elements (see Fig. 1(b)), and the third was also divided into quadrilateral elements and rotated 30 degrees with respect to the x-axis. The mesh is three dimensional, although only the (x, y) plane is shown in the figure. The velocity field is assumed constant at $1ms^{-1}$ parallel to the x-axis on the first two meshes and rotated 30 degrees on the third mesh. This simple case produces a 1D wave front that travels at a constant velocity in the flow direction. Since the problem is physically the same for each case, the choice of element shape and mesh orientation should have no effect on the solution. The computed salinity for each of the above meshes is shown along with the results of the original finite volume method in Fig. 2 at days. The analytical solution is also presented. The figure shows that the results using the DG method are independent of choice of elements and mesh orientation, and show excellent agreement with the analytical solution. The constant approximation finite volume method shows a more smeared wave front due to the artificial viscosity characteristic of first order methods. Fig. 2 also shows the computed temperature distribution at days. At the inflow boundary the temperature remains at 7^0C. The results of the DG method show a sharper drop and, similarly to the salinity results, do not exhibit the smearing of the front as does the finite volume method. Fig. 3 shows the solutions for salinity and temperature, respectively, under mesh refinement in the -direction using the DG method. Also shown in the figures are the solutions using the finite volume method on the most refined mesh ($80 \times 3 \times 1$). The figures show that

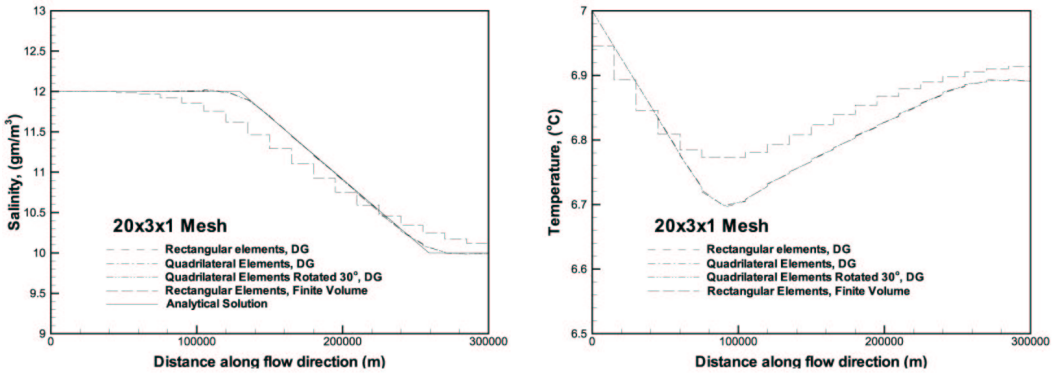

Figure 2. Solution of (left) salinity and (right) temperature for 1D flow at $t = 3$ days on several meshes using linear DG and constant finite volume methods.

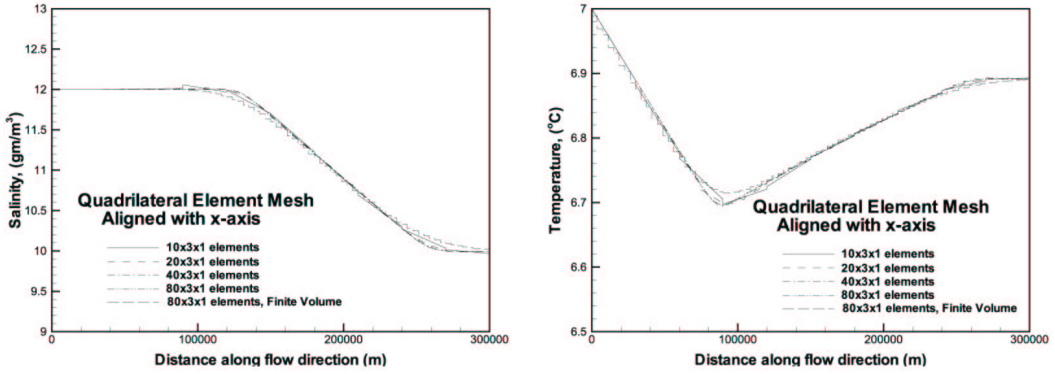

Figure 3. Solution of (left) salinity and (right) temperature for 1D flow at $t = 3$ days under mesh refinement in x direction.

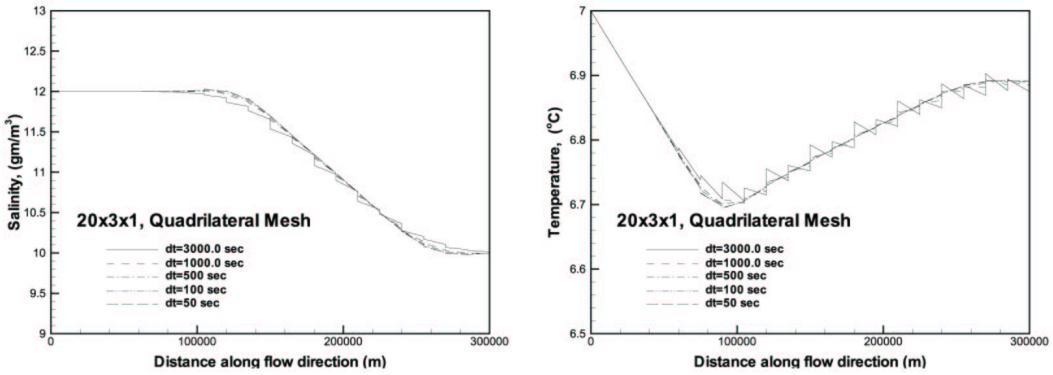

Figure 4. Solution of (left) salinity and (right) temperature for 1D flow at $t = 3$ days under time refinement.

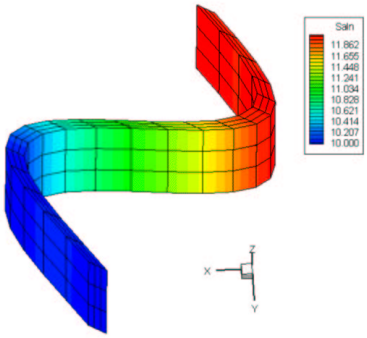

Figure 5. Three day simulation of river flow, concentration contours.

the solution using the DG method is essentially independent of mesh size, except for the $10 \times 3 \times 1$ mesh, which shows some slight overshoot in salinity near the wave front and tail. The figures also indicate that the solution using the finite volume method improves under mesh refinement. However, the solution for salinity is still smeared near the wave front and tail, and the solution for temperature is smoothed near the minimum temperature as compared to the DG method. However, as seen by comparing Fig. 2 and Fig. 3, the DG method produces a more accurate solution on a coarser mesh. A time step sensitivity study was performed on the $20 \times 3 \times 1$ mesh. The results are shown in Fig. 4 for salinity and temperature, respectively. The figures show that the solution converges under time step refinement. For $\Delta t = 3000$, the solution has not yet converged. However, it is seen that for $\Delta t \leq 1000$, the solution becomes insensitive to time step.

5.2. Three dimensional River Study

The next case simulates flow in a river or tributary. The initial and boundary conditions are the same as the previous cases. In the previous cases, the velocity field was constant

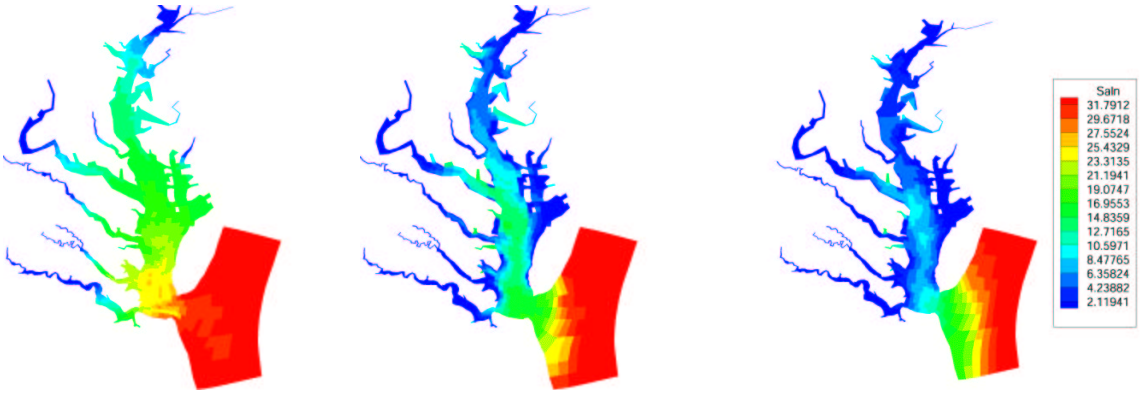

Figure 6. Salinity concentration at selected times (from left to right: $t = 0, 5, 10$ days).

in both magnitude and direction. This case was chosen to test the solution when the velocity vector varies in direction. It is similar to the previous case in the sense that a wave propagates through the domain at the local velocity. However, due to the geometry of the flow, it is fully two-dimensional. Fig. 5 shows salinity contours at days on a $20 \times 3 \times 1$ mesh using a time step sec.

5.3. Chesapeake Bay Model

The salinity and temperature for the Chesapeake bay are computed using constant elements. The initial conditions for the Chesapeake Bay model are non-uniform and given in an input file for each element in the domain. The boundary conditions on salinity are saltwater at ocean boundaries and freshwater at river boundaries. The boundary conditions on temperature specify the temperature of the inflow at all boundaries. These are given in input file. Additionally, the air temperature above the surface varies, providing a heat flux boundary condition at the surface of the domain. The mesh has 2100 surface elements and 10196 total elements. It is divided into 19 layers. Results for salinity and temperature at selected times during the simulation are shown in Fig. 6 and Fig. 7 respectively.

6. Conclusions and Future Work

A Discontinuous Galerkin method for mass conservation equations has been developed and validated. Computational experiments indicate that this approach is robust and can treat sharp fronts. Theoretical results in [11] show that this method can be applied to non-conforming grids which is very important in developing dynamic adaptive algorithms. Present studies include investigating different time stepping schemes as well as treating reactive transport.

REFERENCES

1. F. Bassi and S. Rebay, A high-order accurate discontinuous finite element method for the numerical solution of thecompressible Navier-Stokes equations, J. Computational

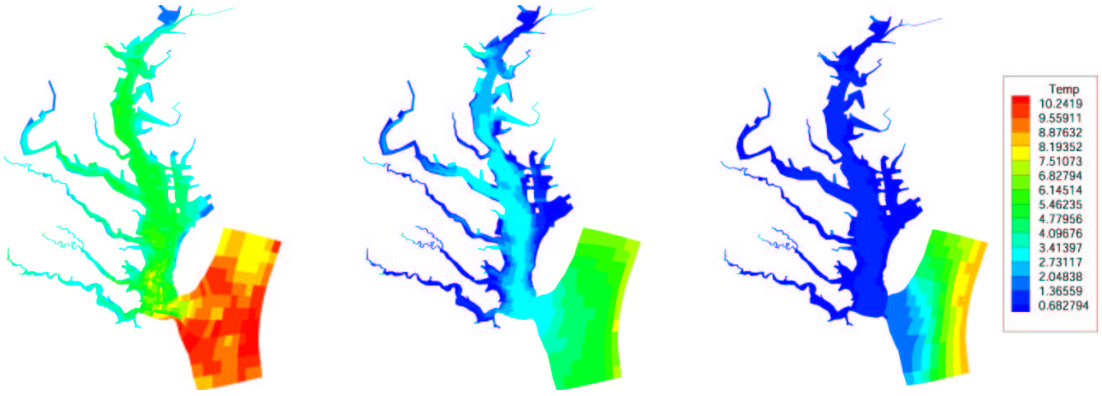

Figure 7. Temperature distribution at selected times (from left to right: $t = 0, 5, 10$ days).

Phys. No. 131(1997), 267.

2. B. Cockburn and C.W. Shu, The local discontinuous Galerkin method for convection-diffusion systems, SIAM J. Numer. Anal. No. 35 (1998), 2440.
3. J.T. Oden, I. Babuska and C.E. Baumann, A discontinuous hp finite element method for diffusion problems, Journal of Computational Physics No. 146 (1998) 491.
4. M.F. Wheeler, An elliptic collocation-finite element method with interior penalties, SIAM J. Numer. Anal. No. 15 (1978) 152.
5. J. Douglas and T. Dupont, Interior penalty procedures for elliptic and parabolic Galerkin methods, Lecture Notes in Physics 58, Springer-Verlag, Berlin, (1976).
6. B. Riviere, M.F. Wheeler and V. Girault, V., Improved energy estimates for interior penalty, constrained and discontinuous Galerkin methods for elliptic problems. Part I., Computational Geosciences No. 3 (1999), 337.
7. B. Riviere, M.F. Wheeler and V. Girault, A priori error estimates for finite element methods based on discontinuous approximation spaces for elliptic problems, SIAM J. Numer. Anal. No. 39 (2001) 902.
8. D. Arnold, F. Brezzi, C. Cockburn and D. Marini, Discontinuous Galerkin methods for elliptic problems, First International Symposium on Discontinuous Galerkin Methods, Cockburn, B., Karniadakis, G.E. and Shu, C.W., eds., Lecture Notes in Computational Science and Engineering, Springer-Verlag, No. 11 (2000), 89.
9. First International Symposium on Discontinuous Galerkin Methods (B. Cockburn,G.E. Karniadakis and C.W. Shu, eds.), Lecture Notes in Computational Science and Engineering, Springer-Verlag, No. 11 (2000).
10. C. Cerco and T. Cole, Users Guide to the CE-QUAL-ICM 3-D Eutrophication Mode, U.S. Army Corps of Engineers, Waterways Experiment Station., Technical Report EL-95-15 (1995).
11. B. Rivière and M.F. Wheeler, Nonconforming methods for transport with nonlinear reaction, Proceedings of the Joint Summer Research Conference on Fluid Flow and Transport in Porous Media, to appear.